

GEOLOGY AND NATURAL RESOURCES OF NIGERIA

Edited by
Silas S. Dada, Samuel B. Olobaniyi,
and Kamaldeen O.L Omosanya

CRC Press
Taylor & Francis Group

12 Archean Zircon Xenocrysts and Timing of Gold Mineralization in Nigerian Schist Belts

Silas S. Dada, Jimoh Ajadi, Abdulrazaq A. Garba, Ifeanyi A. Oha, Naheem Banji Salawu, and Paulinus N. Nnabo

HIGHLIGHTS

- The occurrence of xenocryst zircon cores with Paleoarchean model ages in Alagbede goldfield confirms that southwestern Nigeria is underlain by rocks of great antiquity.
- A Pan-African age of between 617 and 563 (590+27) Ma is proposed as the period of gold mineralization in Alagbede.
- The timing of the gold mineralization is related to the formation of structural lineaments and felsic magmatism.
- A two-phase gold mineralization is proposed with an earlier Birimian/Eburnean and a later epigenetic Pan-African dispersal/amalgamation phase in the West Gondwana mobile belts with obvious consequences on mineral deposit preservation.

12.1 INTRODUCTION

Alagbede auriferous district is in the northwestern part of the crystalline basement of southwestern Nigeria in a region underlain by the migmatite-gneiss complex, overlain by Proterozoic metasediments (Figure 12.1) including massive and foliated quartzite, quartz-mica schist, meta-ultramafite represented by the talc-tremolite-actinolite schist; intruded by various granitic suites. The granitoids range from porphyroblastic granite, porphyritic granite, porphyritic diorite, medium- to coarse-grained alkali granite, medium-grained granodiorite, alkali syenite, pegmatite/aplite and vein quartz (Figure 12.2). Located east of the Igbetti carbonate-quartzite-schist belt and south of the Yauri goldfield, it has been regarded as an Eburnean terrain, having been reworked by at least two episodes of granite plutonism (Rahaman et al., 1983) with evidence of significant alkaline magmatism. The absence of systematic exploration and development in the study area has resulted in intense artisanal workings which target both the primary gold-quartz reefs and their associated alluvial occurrences.

Although several earlier studies carried out on primary gold deposits within the Nigerian schist belts have related the mineralization to structural lineaments associated with periods of felsic magmatism, thereby inferring the timing of the gold mineralization to the time of such magmatic activities, there has been no record of any attempt to date or establish the age of the gold mineralization event. Alagbede gold deposit is spatially related to vein quartz, fine-grained syenogranite and talc schist (Ajadi et al., 2018) and the determination of its actual time of mineralization would lead to a

DOI: 10.1201/9781003454908-12

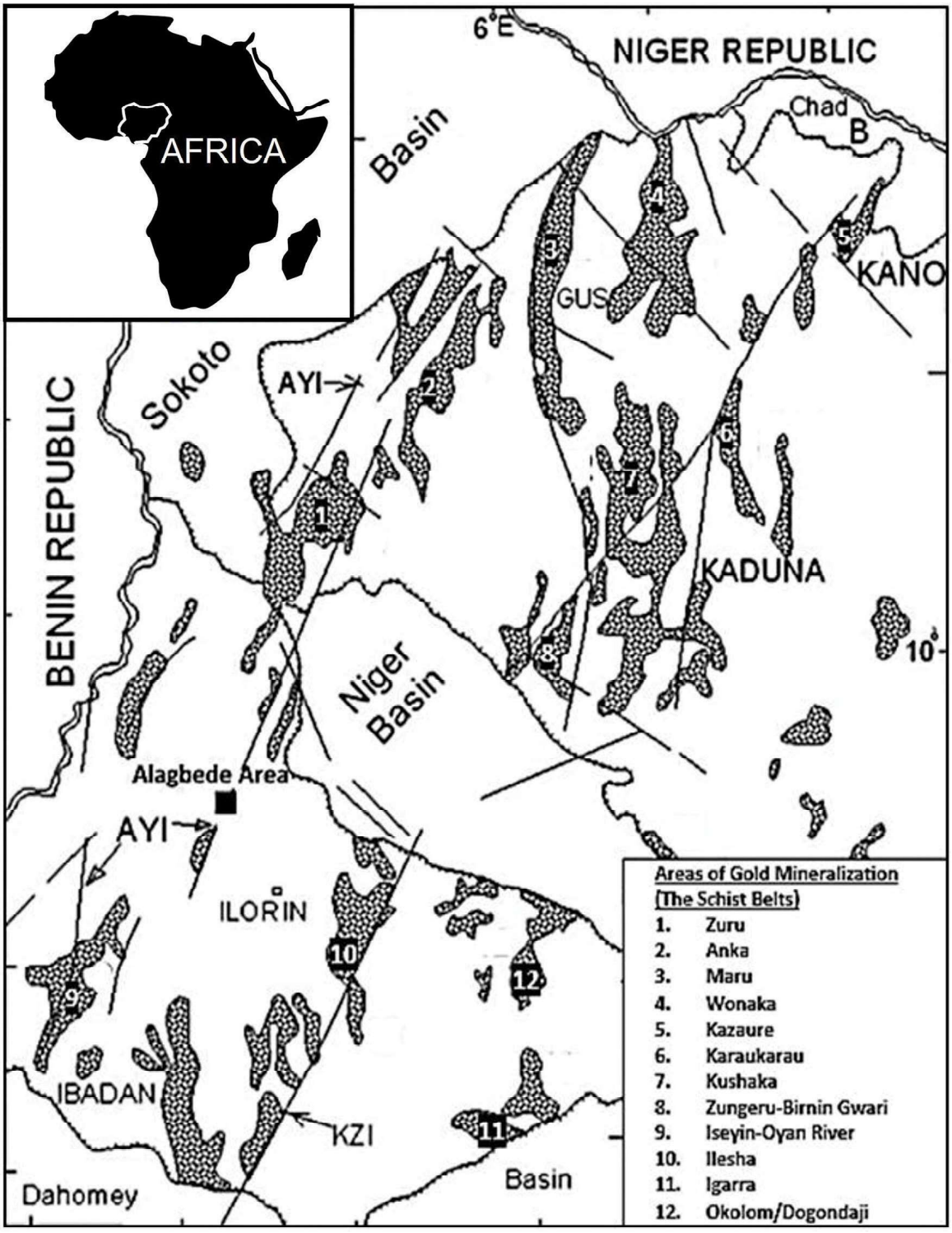


FIGURE 12.1 Simplified Geological map of Nigeria showing the schist belts, the study area (black square) in a generalised geological map of western part of Nigeria showing the major areas of gold mineralization in relation to major transcrustal (Anka-Yauri-Iseyin – AYI) and (Kalangai-Zuru-Ifewara - KZI) faults. (After Woakes et al., 1987 and Garba, 2003.)

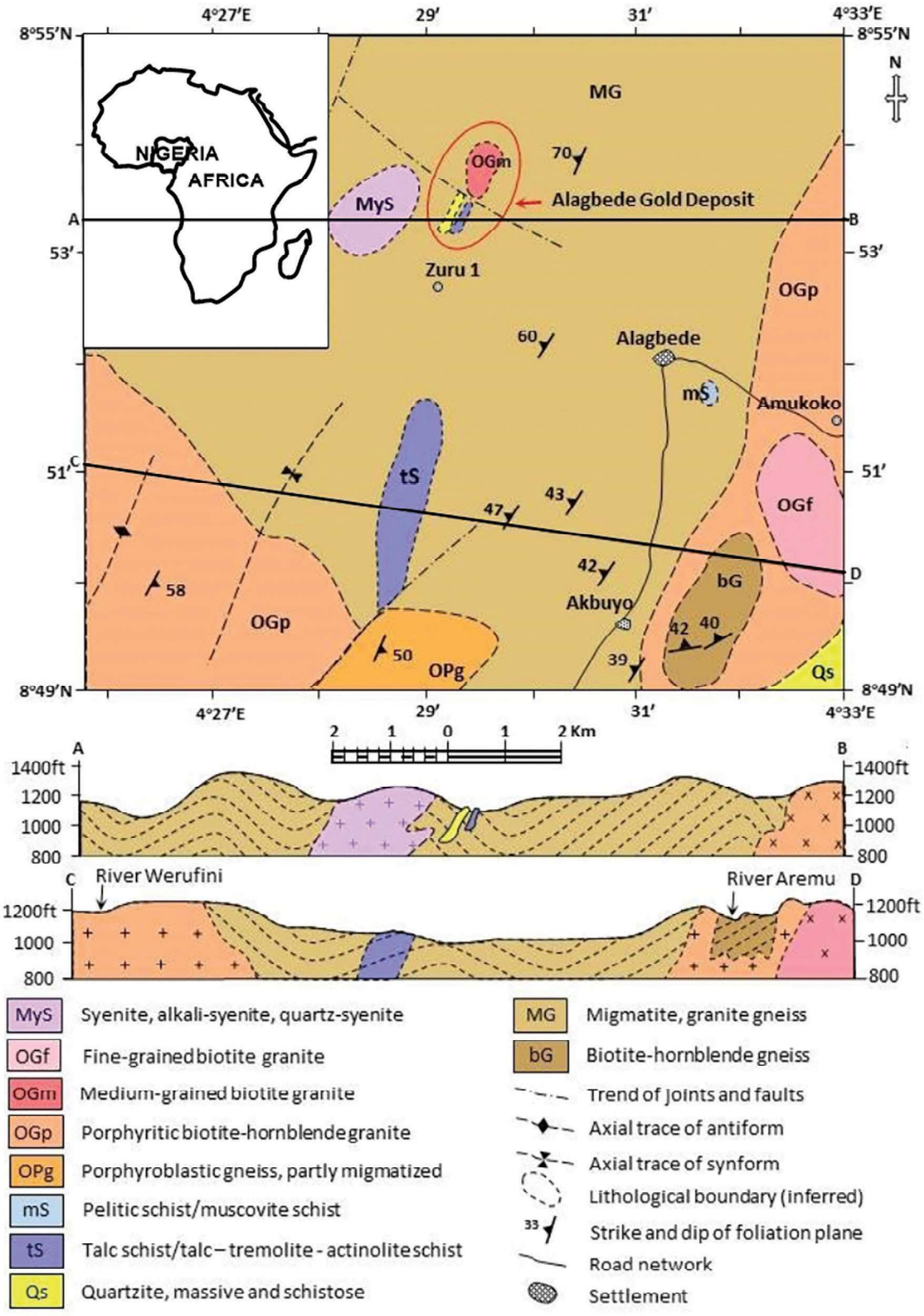


FIGURE 12.2 Geological map of Alagbede area with gold deposit zone in red circle and Figure 12.1 as inset.

better assessment of the economic potential of host felsic intrusions, assist gold exploration in the area and in the Nigerian schist belts. The primary deposits are being exploited by artisanal miners mainly in the southern segment of the main quartz vein which forms a NNE-SSW-striking belt, extending locally for 500 m with a width ranging from 20 to 50 m. Located about twenty kilometers north of Alagbede is Kursi Mines; a large-scale mechanized working which commenced a few years ago. This study, which includes U-Th-Pb zircon dating has been carried out using the Laser Ablation Inductively Coupled Plasma-Mass Spectrometry (LA-ICP-MS) for the purpose of determining the age of the gold mineralization event, while the use of associated sulfides (Figure 12.3) in the vein quartz (arsenopyrite, galena, pyrite and pyrrhotite) is envisaged for the future.

12.2 ANALYTICAL PROCEDURE

12.2.1 Microanalysis

A combination of Electron Probe Micro Analyses (EPMA), Scanning Electron and Cathodoluminescence (SEM-CL) microanalyses were carried out on zircons from all samples meant for analysis with a first order (Figure 12.4) textural classification of zircons, which resulted in the following groups:

- **Xenocrystic Inherited Zircons:** These are zircons recovered from the rocks that show inherited core and exhibit growth zoning (oscillatory zoned core) with local intermediate resorption of magmatic zircons. The cores are locally overprinted by zones of recrystallization (re-homogenization) in which the original euhedral zircon has been cut by rapidly recrystallized or newly grown domains of more homogeneous composition.
- **Magmatic Zircon:** These are mostly seen as small euhedral zircons with oscillatory growth zoning that are masked by re-homogenization at the rims while some are completely recrystallized and partly fragmental. Some of the locally resorbed magmatic zircons show hydrothermal alteration at the rims and dissolution structure.
- **Metamorphic Zircons:** These zircons are mostly homogeneous, un-zoned and fragmental but some exhibit ghost xenocrystic core and hydrothermal alteration at the rims.
- **Eclogitic Zircon**: were observed to be replacing and rimming the pre-metamorphic phase.

The selected grains of zircon for each of the rock samples were size-graded and arranged in an ordered manner on double-sided adhesive tape fixed onto glass slides. Each group of zircon grains picked from the same sample was photographed and assigned the sample identification number for easy correlation when required after mounting. Measurement of sizes and shapes of the grains were made before they were placed in special molds and encased in blocks of epoxy resin. A standard polishing technique was maintained to expose the details of the internal variation, particularly the presence of zoning and inclusions in the grains. The size-grading of the zircon grains before mounting was done to ensure that each grain was cut and exposed by half its original width as much as possible before they were finely polished and carbon-coated for EPMA. The studied felsic plutonic rocks from Alagbede area contain well preserved, euhedral to subhedral, colorless to pinkish prismatic zircons. The abundance of zircon and the sizes of grains vary between samples. The quartz porphyritic volcanic rock contains abundant zircons with many relatively large grains while the alkali granite shows smaller but euhedral zircon grains. The microprobe instrument uses a very fine beam of electrons to generate X-rays which makes possible, in situ chemical analyses of spots in the grain around 1μm diameter as well as any other mineral inclusions. The electron microprobe was used to study and characterize the internal variation within zircon grains. The finely polished and carbon-coated zircon and rock thin sections were examined in detail using the scanning electron microscope to identify common variation in phases of mineral growth that had taken place and particularly which minerals had formed during the same mineralization events

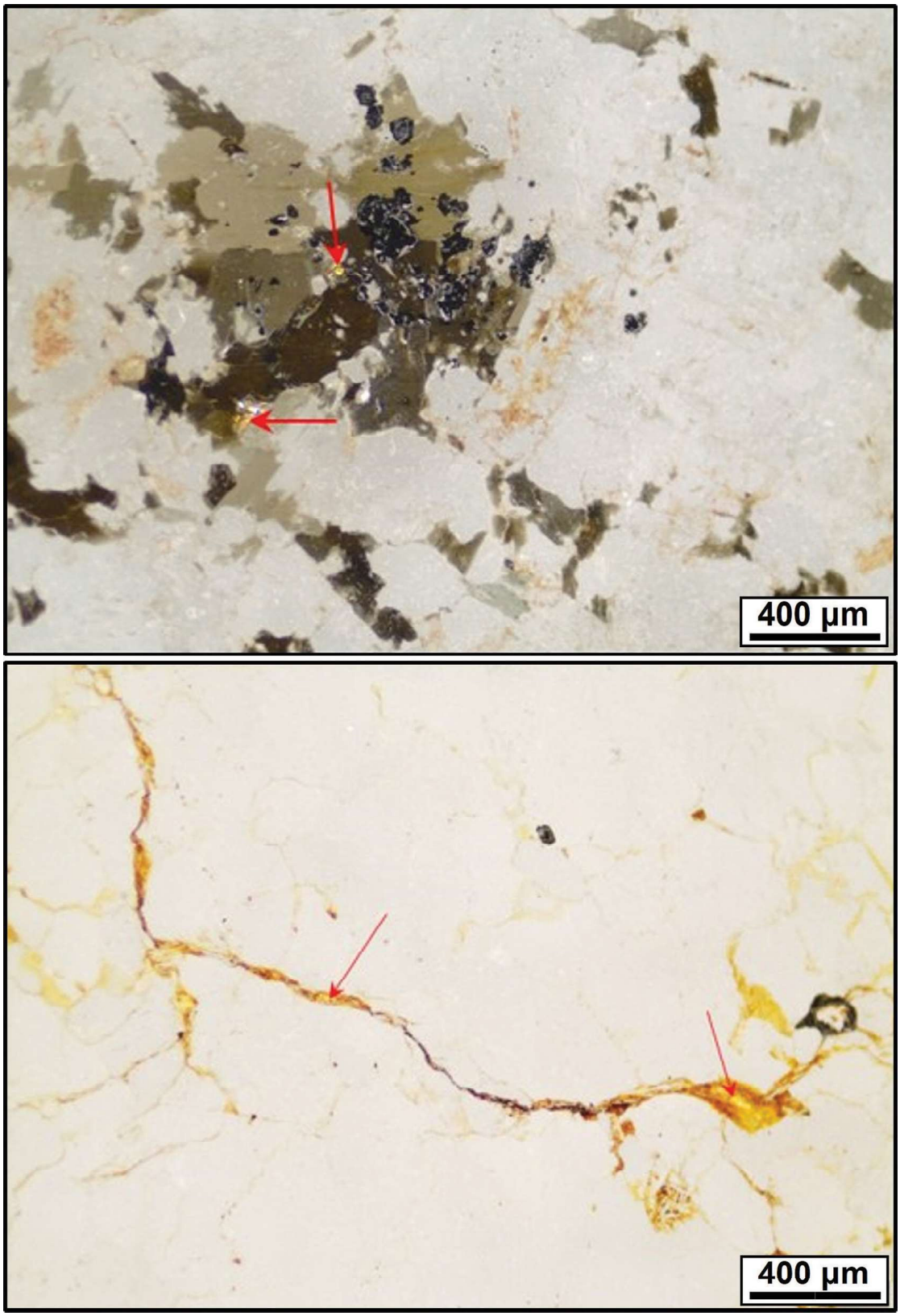


FIGURE 12.3A Occurrence of small free gold in syenogranite (top) and microfracture-filling gold inclusions within the vein quartz (bottom).

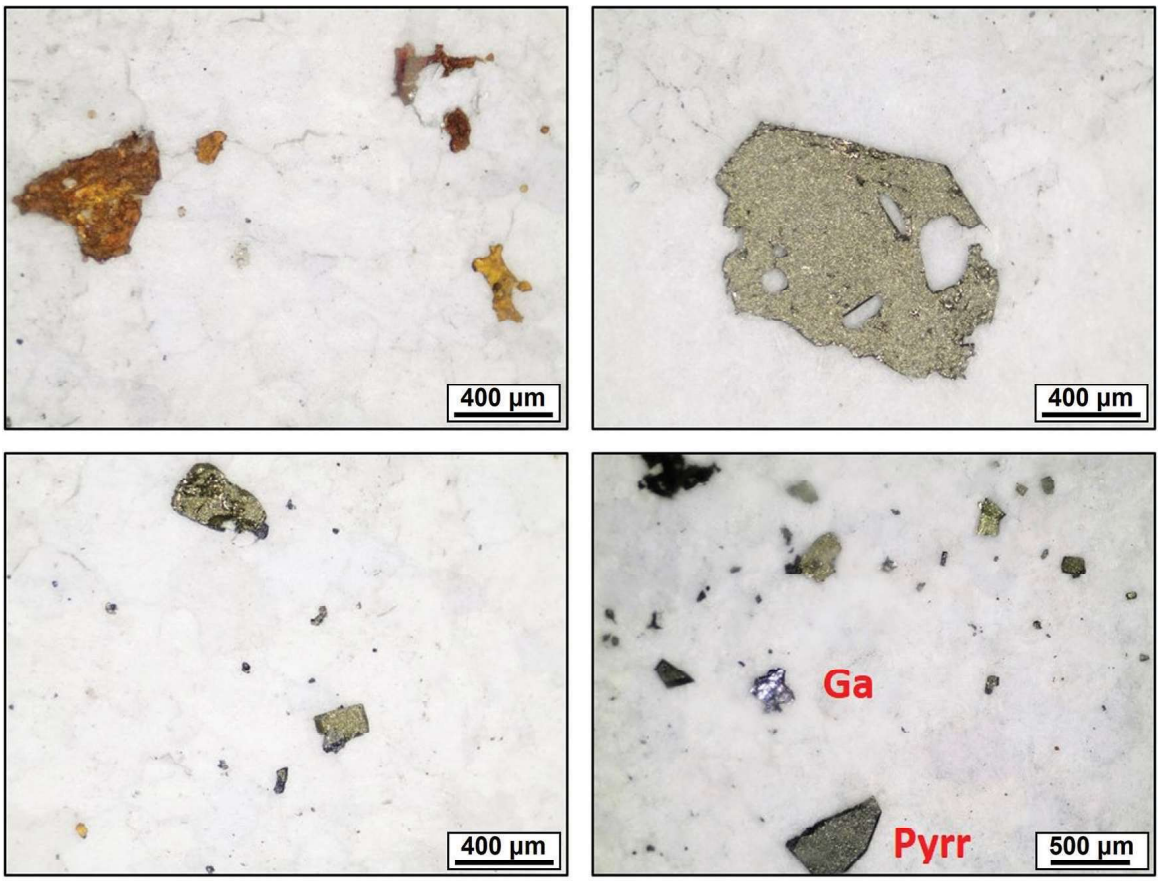


FIGURE 12.3B Inclusions of sulfide mineralization within the vein quartz (Ars = arsenopyrite, Ga = Galena, Py = pyrite, Pyrr = pyrrhotite).

as the gold. Prior to LA-ICPMS analysis, Cathodoluminescence (CL) images of all crystals were obtained (Figures 12.4–12.7) to avoid apatite and potassium feldspar inclusions as well as cracks and fissures during analysis.

The geochemical and structural variations within a crystal determine the intensity of SEM-CL emissions, thus making this technique suitable for structural, textural and compositional examination for any given sample. In this study, cathodoluminescence (CL) images were taken with VEGA3 TESCAN equipped with an X-Max energy-dispersive spectrometer (EDS) and used to examine the internal structure of individual zircon grains in order to ensure good spot selection for laser analytical work as well as to evaluate minerals for heterogeneous growth (complex history, overgrowths, dissolution and crack infilling). Therefore, SEM-CL imaging was used as a tool to delineate sequential episodes of quartz precipitation and define the paragenetic sequences of hydrothermal vein sets as suggested by Bernet and Bassett (2005).

12.2.2 Geochronology – Laser Ablation ICP-MS U-Th-Pb Zircon Dating

Zircon grains for U-Th-Pb dating were extracted from seven rock samples by heavy-liquid and magnetic separation, and further hand-picked under a binocular microscope before mounting, cutting, polishing and carbon-coating of zircon grains preparatory to microprobe and laser ablation studies. Having concluded on the close association of the gold and the sulfides, zircon grains closely associated with them from petrographic and SEM studies were separated from seven of the rock units for the purpose of studying the evolution of the continental crust and related metallogeny in the area.

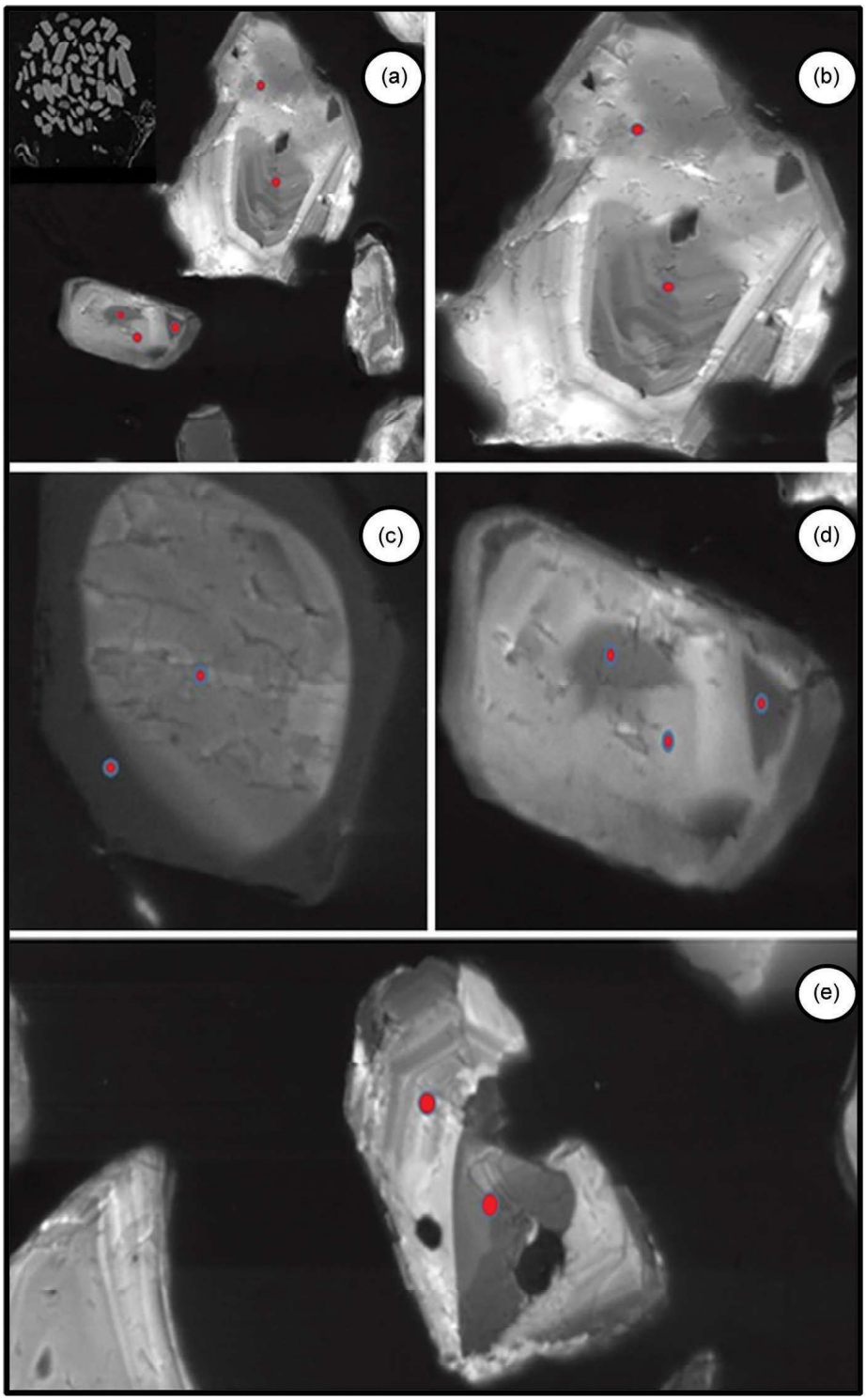


FIGURE 12.4 (a–e) Cathodoluminescence images of zircons in medium-grained alkali granite.

12.3 RESULTS

Total U, Th and Pb concentrations and isotopic compositions/ratios of zircon grains extracted from seven (7) different rock samples from Alagbede area were measured (Table 12.1), analyzed and interpreted and presented below (Figures 12.8–12.11). Unlike traditional common lead contamination corrections in zircons used for U–Pb geochronology, the analytical method deployed in this

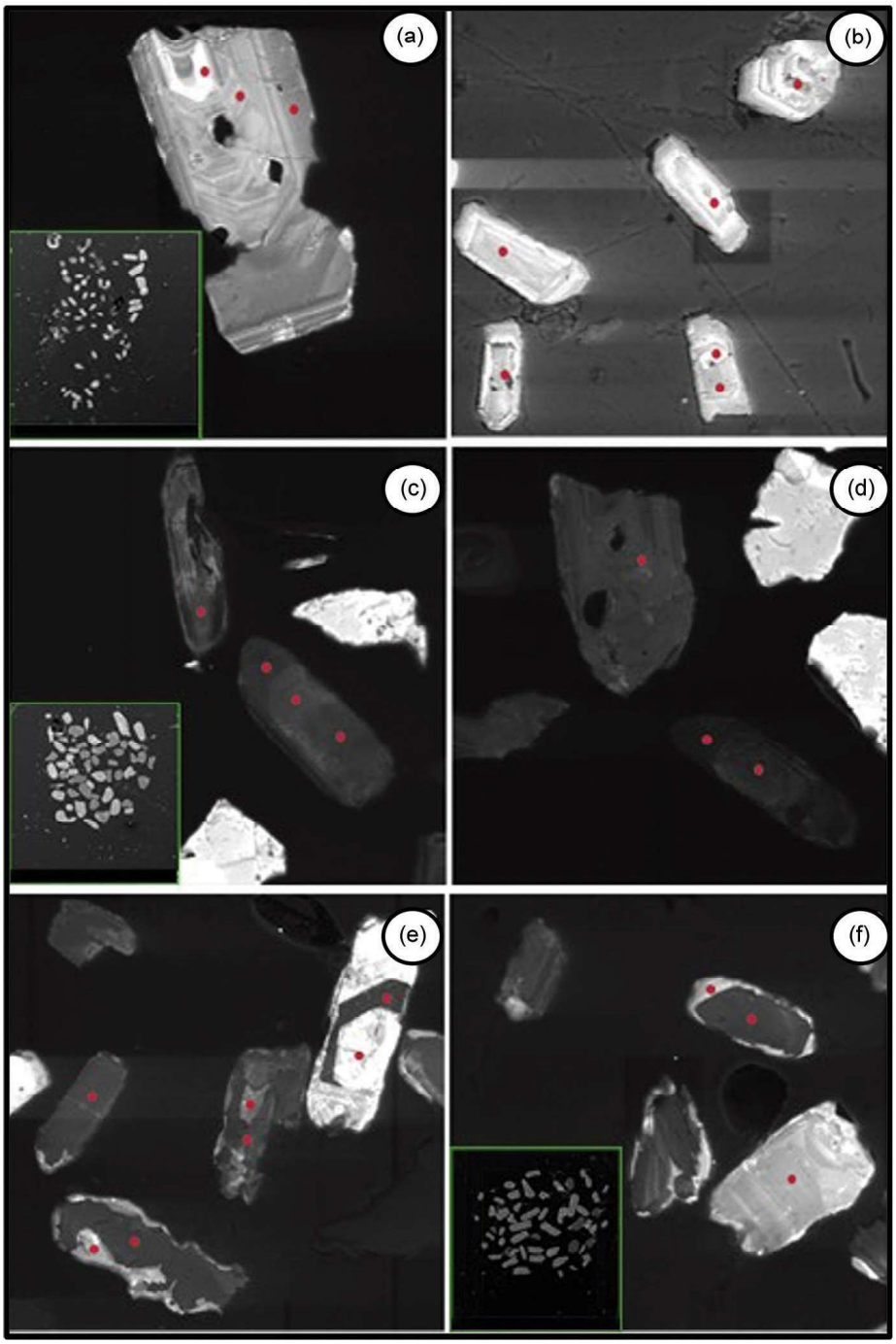


FIGURE 12.5 Cathodoluminescence images of zircons in porphyroblastic granite (a and b), syenite (c and d), and granodiorite (e and f).

study (LAM-ICPMS) does not report ^{204}Pb. Rather, using Andersen's (2002) equations, especially for metamorphic discordant zircons (Mezger and Krogstad, 1997), the method leads to a robust numeric solution using a set of equations relating the content of radiogenic lead in a zircon to its total lead content, the amount of common lead present, the age of initial crystallization, the age of lead loss and the amount of lead lost in that process.

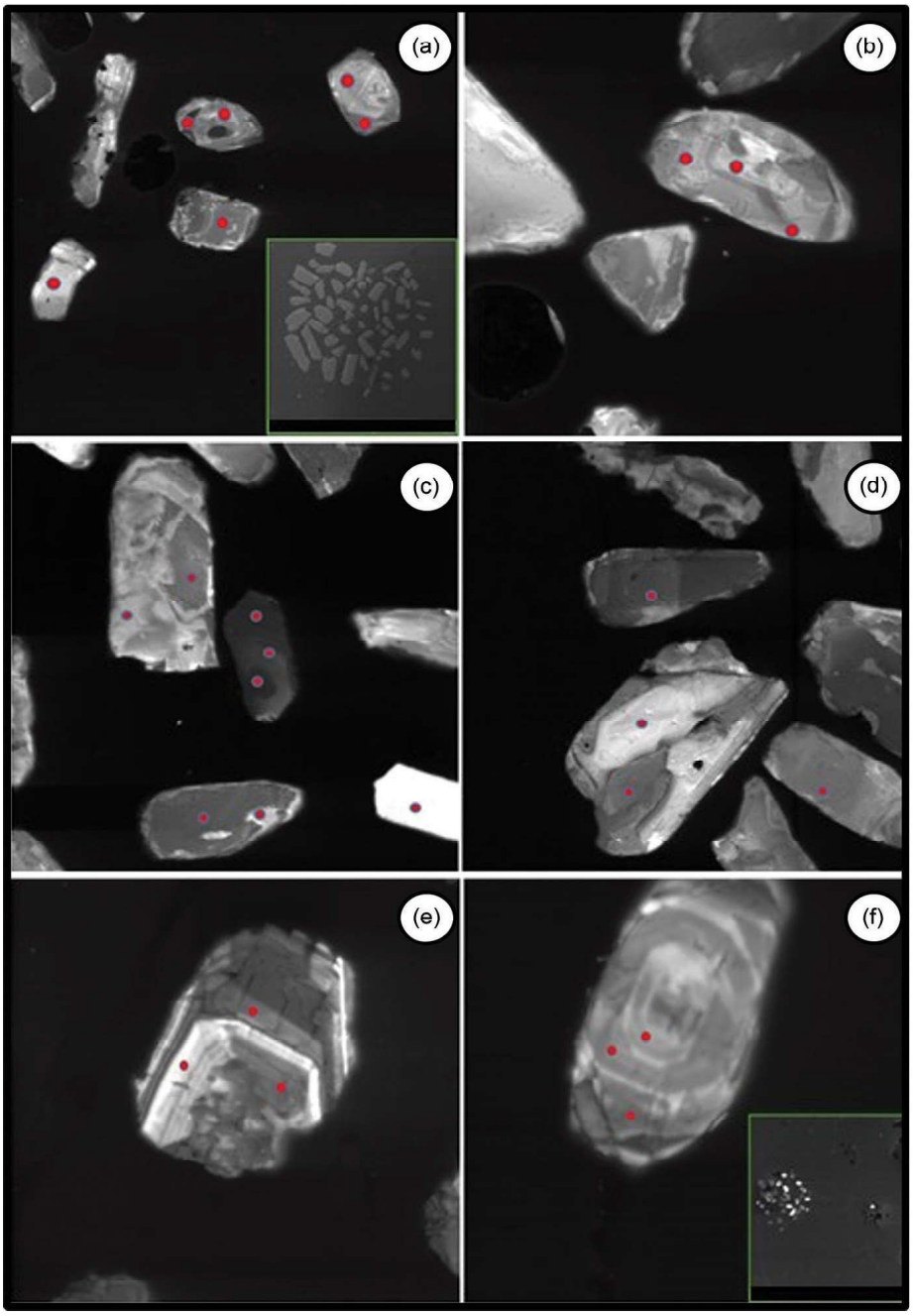


FIGURE 12.6 Cathodoluminescence images of zircons in pegmatite and vein quartz.

12.3.1 Alkali Granite

$^{207}Pb/^{206}Pb$ data analysis of single zircons from alkali granite (sample AG 34) yielded model ages of 3750+270 and 3320+180 Ma after applying the Andersen (2002) common Pb correction These are Archean inherited ages of the xenocrystic cores. The weighted average of the corrected $^{207}Pb/^{206}Pb$ ages after identifying the various age clusters on the probability density plot (Figure 12.8a) are 1746+110, 1221+160 and 590+45 Ma. The non-definition of the crystallization age due to a high degree of discordance by Pb loss especially toward the upper intercept is evident in Figure 12.8b.

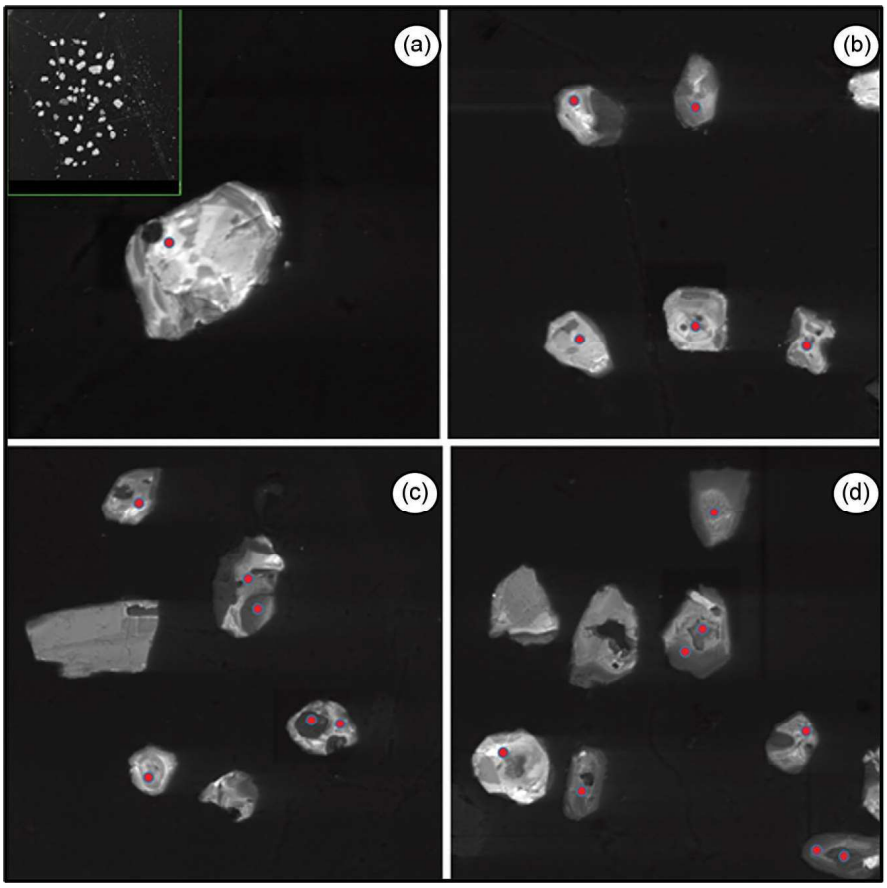


FIGURE 12.7 (a–d) Cathodoluminescence images of zircons in syeno-granite.

12.3.2 Porphyritic Granite

Single zircon $^{207}Pb/^{206}Pb$ model age values of 3780+260 and 3130+170 Ma obtained (Figure 12.8c) are interpreted as corresponding to Archean inherited xenocrystic cores. The mid-Proterozoic ages of 1771+200 Ma on the weighted average plot (Figure 12.8c) and the upper intercept age of 1800+73 Ma on the $^{206}Pb/^{238}U$ versus $^{207}Pb/^{235}U$ Concordia plot represent the age of magmatism that accompanied the Eburnean event whose clocks were reset by tectonism and metamorphism.

12.3.3 Syenite

A single zircon $^{207}Pb/^{206}Pb$ model age of 3520+98 Ma is interpreted as the magmatic age of the xenocrystic zircon core. The $^{207}Pb/^{206}Pb$ weighted mean age plots (Figure 12.9a) of 1740+250 Ma, 1381+290 and 542+75 Ma respectively as well as the probability density plot of the $^{207}Pb/^{206}Pb$ zircon ages show clusters around 1800, 1300 and 500 Ma. The high dispersal of experimental points on the Concordia diagram around both upper and lower intercepts due to Pb diffusion has resulted in the poor definition of both crystallization (1722±59 Ma) and metamorphic (507±100 Ma) respectively.

12.3.4 Granodiorite

Zircons recovered from granodiorite gave a poorly defined single zircon $^{207}Pb/^{206}Pb$ Eburnean age of 2010+170 Ma which is interpreted as the age of magmatism that produced the granodioritic melt which formed the rock. The $^{207}Pb/^{206}Pb$ weighted mean age plot gave 1800+300 and 543+16 Ma

TABLE 12.1
Summary of U-Th-Pb Isotopic Data for Alagbede Goldfield Samples

Zircon ID No.	207Pb/ 235U	% Error	206Pb/ 238U	% Error	Error Correl. (rho)	208Pb/ 232Th	% Error	207Pb/ 206Pb	% Error	207Pb/ 235U Age	% Error	206Pb/ 238U Age	% Error	208Pb/ 232Th Age	% Error	207Pb/ 206Pb Age	% Error
a: Alkali Granite																	
34_52_1	9.4	2.0	0.216	0.034	0.92028	0.0818	0.0079	0.291	0.026	2170	200	1300	170	1580	150	3320	180
34_6_1	16.6	5.2	0.38	0.10	0.91977	0.219	0.057	0.381	0.061	2830	370	2000	430	3870	930	3750	270
b: Porphyritic Granite																	
44_5_1	2.21	0.72	0.1026	0.0096	0.64171	0.086	0.018	0.022	0.022	1070	120	627	55	1720	290	2010	250
44_3_1	1.63	0.22	0.0864	0.0072	0.25484	0.068	0.012	0.017	0.017	946	82	533	43	1310	230	2060	250
44_2_1	4.63	0.86	0.133	0.020	0.7797	0.42	0.23	0.023	0.023	1640	160	790	110	-	-	3130	170
44_21_1	20.7	8.6	0.39	0.12	0.95435	-1.6	2.3	0.068	0.068	2990	370	2020	540	-	-	3780	260
c: Syenite																	
55_13_1	4.55	0.16	0.3099	0.0046	0.20766	0.0850	0.0034	0.1075	0.0030	1735	29	1740	23	1648	63	1748	49
55_34_1	4.090	0.074	0.2728	0.0026	0.55785	0.0743	0.0012	0.1077	0.0017	1649	15	1555	13	1449	23	1753	28
55_5_1	4.71	0.19	0.3094	0.0035	0.22375	0.0825	0.0024	0.1114	0.0038	1763	33	1737	17	1602	44	1808	57
55_23_1	2.70	0.43	0.132	0.011	0.703	0.089	0.010	0.150	0.020	1270	120	812	65	1710	190	2100	260
55_20_1	9.6	1.9	0.202	0.024	0.94125	0.63	0.18	0.319	0.022	2240	160	1200	140	-	1500	3520	98
d: Granodiorite																	
57_53_3	4.77	0.11	0.3113	0.0029	0.47465	0.0822	0.0016	0.1113	0.0021	1790	22	1771	19	1648	38	1812	37
57_8_1	3.63	0.24	0.254	0.010	0.94321	0.0669	0.0050	0.1002	0.0036	1774	20	1747	14	1595	30	1814	33
57_40_1	3.07	0.57	0.145	0.016	0.7896	0.137	0.070	0.139	0.014	1240	110	855	86	2700	1100	2010	170

(*Continued*)

TABLE 12.1 (*Continued*)
Summary of U-Th-Pb Isotopic Data for Alagbede Goldfield Samples

Zircon ID No.	207Pb/ 235U	% Error	206Pb/ 238U	% Error	Error Correl. (rho)	208Pb/ 232Th	% Error	207Pb/ 206Pb	% Error	207Pb/ 235U Age	% Error	206Pb/ 238U Age	% Error	208Pb/ 232Th Age	% Error	207Pb/ 206Pb Age	% Error
e: Pegmatite																	
62_46_1	4.37	0.16	0.3056	0.0055	0.66635	0.0822	0.0018	1856	36	1815	20	1783	15	1577	29	1856	36
62_33_1	4.62	0.11	0.3108	0.0042	0.47655	0.0834	0.0018	1865	38	1828	25	1805	23	1659	49	1865	38
62_1_2	4.45	0.10	0.2963	0.0029	0.53296	0.0819	0.0012	1869	40	1737	23	1630	16	1437	41	1869	40
62_8_1	4.770	0.098	0.3092	0.0034	0.36018	0.0792	0.0012	1884	31	1775	17	1682	15	1538	28	1884	31
62_11_1	3.89	0.15	0.2704	0.0047	0.78848	0.0737	0.0022	2250	250	907	97	455	50	1020	250	2250	250
f: Vein quartz																	
81-12_1	0.780	0.013	0.09720	0.00059	0.41564	0.0313	0.0021	0.05866	0.00062	584.3	7.2	597.9	3.5	622	42	552	22
81-14_2	0.7829	0.0092	0.09541	0.00057	0.32769	0.0281	0.0032	0.05952	0.00046	587.4	5.1	587.4	3.3	556	64	583	17
81_14_1	0.7945	0.0096	0.09730	0.00059	0.57566	0.02470	0.00025	0.05968	0.00017	593.2	5.5	598.5	3.5	493.1	4.9	591.7	6.2
81_11_2	0.805	0.012	0.09773	0.00056	0.29052	0.0291	0.0023	0.05995	0.00065	599.1	6.7	601.0	3.3	578	45	596	24
81_23_1	0.856	0.026	0.1011	0.0015	0.87698	0.068	0.018	0.0613	0.0013	625	14	620.6	8.7	1240	310	628	47
g: Alkali granite (syenogranite)																	
85_34_1	0.732	0.011	0.08984	0.00070	0.60054	0.02671	0.00072	0.05878	0.00063	557.0	6.5	554.6	4.1	533	14	553	24
85_41_2	0.756	0.011	0.09285	0.00060	0.5606	0.0285	0.0013	0.05877	0.00056	570.9	6.3	572.4	3.5	567	26	554	21
85_39_1	0.740	0.012	0.09090	0.00084	0.57754	0.02624	0.00071	0.05922	0.00058	561.6	7.3	560.8	4.9	523	14	574	21
85_46_1	0.689	0.034	0.0821	0.0030	0.88665	0.0352	0.0030	0.0601	0.0013	526	20	508	18	697	58	583	52
85_7_1	0.817	0.014	0.1000	0.0011	0.85152	0.02646	0.00046	0.05948	0.00039	605.2	7.8	614.5	6.5	527.8	9.0	585	15

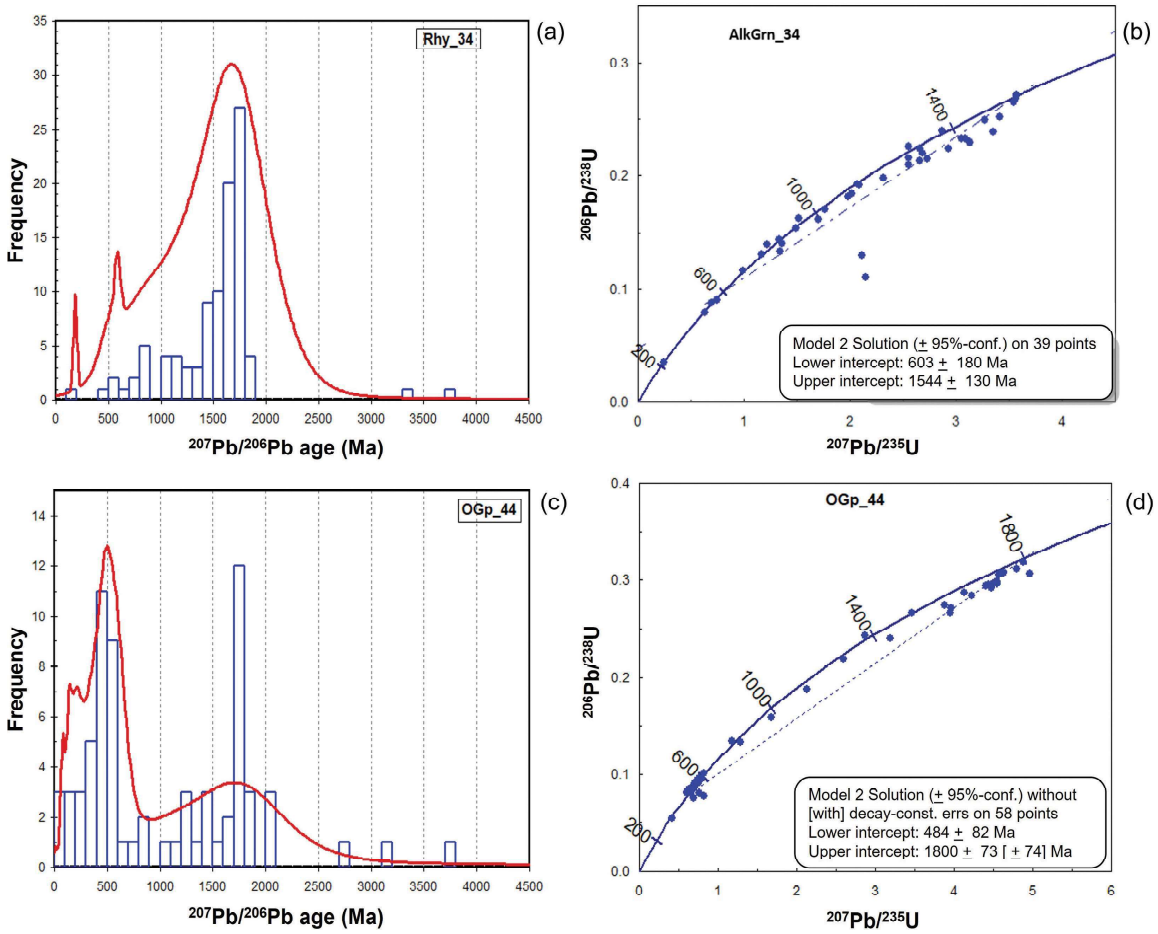


FIGURE 12.8 (a) Probability frequency diagram for zircon ages and (b) $^{206}Pb/^{238}U$ versus $^{207}Pb/^{235}U$ Concordia plot for zircons from alkali granite. (c) Probability frequency diagram for zircon ages and (d) $^{206}Pb/^{238}U$ versus $^{207}Pb/^{235}U$ Concordia plot for zircons from porphyritic granite.

respectively, based on the groupings on the age-frequency probability histogram (Figure 12.9c). They are both coherent with the upper and lower intercept ages of 1869±87 and 570±47 Ma which represent the late Eburnean and Pan-African events respectively on the Concordia plot (Figure 12.9d).

12.3.5 Pegmatite

A single zircon $^{207}Pb/^{206}Pb$ model age of 2250+250 Ma obtained from the pegmatite sample is interpreted as the age of a xenocrystic zircon formed in the Early Proterozoic. It represents key evidence of the Eburnean age of its protolith. The $^{207}Pb/^{206}Pb$ weighted mean average plots for zircon ages gave 1760+71, 1198+160 and 566+59 Ma. The probability density plot (Figure 12.10a) of the $^{207}Pb/^{206}Pb$ zircon ages shows clusters around 1800, 950 and 550 Ma.

12.3.6 Vein Quartz

Zircon U-Th-Pb data for the gold-bearing vein quartz which when plotted on the frequency probability plot (Figure 12.10c) shows an age cluster around 550 Ma but on the $^{206}Pb/^{238}U$ versus $^{207}Pb/^{235}U$ Concordia (Figure 12.10d) gave a Pan-African age of 583+19 Ma with an upper intercept age of 1330+35 Ma. The prominence of the Pan-African event in the formation of the vein quartz is affirmed.

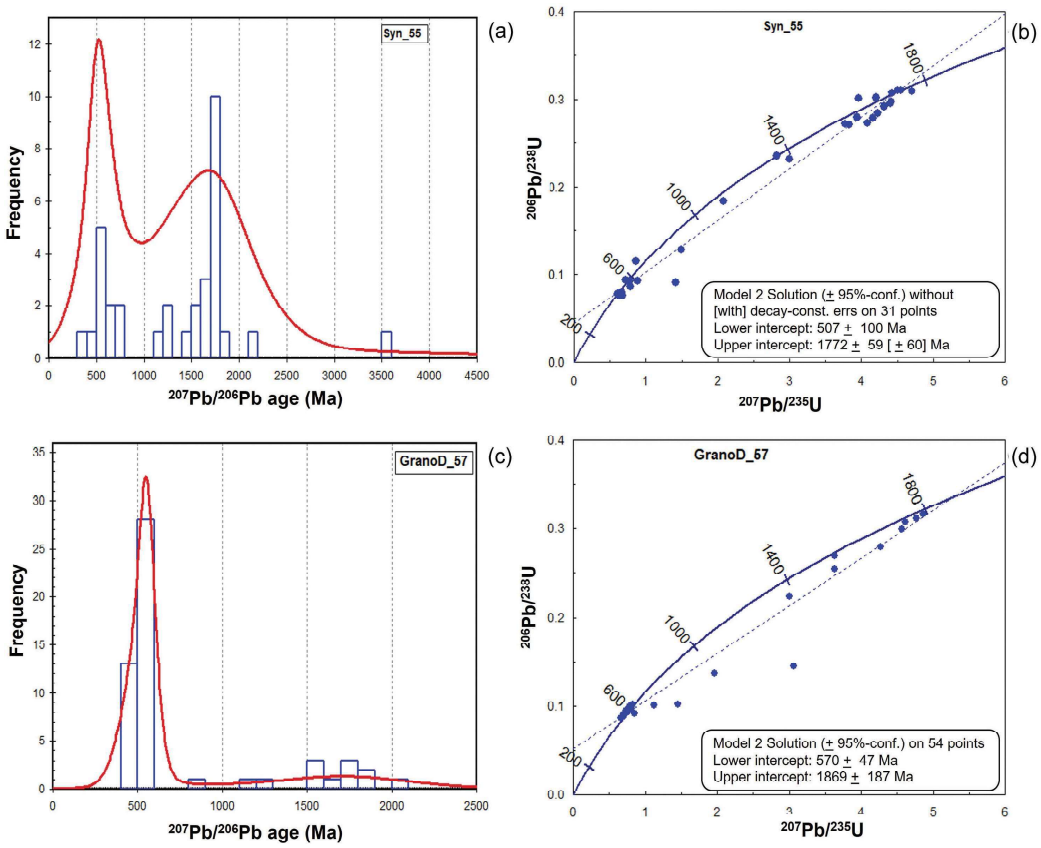


FIGURE 12.9 (a) Probability frequency diagram for zircon ages and (b) $^{206}Pb/^{238}U$ versus $^{207}Pb/^{235}U$ Concordia plot for zircons from syenite. (c) Probability frequency diagram for zircon ages and (d) $^{206}Pb/^{238}U$ versus $^{207}Pb/^{235}U$ Concordia plot for zircons from granodiorite.

12.3.7 Alkali Granite (Syenogranite)

U-Th-Pb data for alkali granite (syenogranite) yielded a Pan-African weighted age of 596+28 Ma (Figure 12.11a) with xenocrystic core indications of between 1500 and 1250 Ma. Age-frequency probability histogram also shows a cluster around 480 Ma while the $^{206}Pb/^{204}Pb$ versus $^{238}U/^{204}Pb$ Concordia plot (Figure 12.11b) yielded an isochron age of 584+49 Ma around a strongly discordant Pan-African event between 600 and 600 Ma with a lower intercept age of 575+17 Ma and an upper intercept age of 2416+360 Ma.

12.4 DISCUSSION

12.4.1 Evolution of Gold Mineralization in the Study Area

We interpret the imprecise weighted average age of 1746+110 Ma of the alkali granite (AG 34) as the imprints of the late Eburnean thermotectonic magmatism (Figure 12.8a). Its weighted average age of 590+45 is consistent with 603+180 Ma lower intercept age obtained on the $^{206}Pb/^{238}U$ versus $^{207}Pb/^{235}U$ Concordia plot (Figure 12.8b), within their error margins. This is considered as indicating the age of the magmatic emplacement during the Pan-African thermotectonic event. The mid-Proterozoic age range of 1771–1800+73 Ma, obtained for the porphyritic granite, on the Concordia (Figure 12.8d) represents the age of magmatism that accompanied the Eburnean thermotectonic event while the weighted mean age of 527+41 Ma and the lower intercept age of 484+82 Ma, which is slightly low as a result of Pb loss by the zircons, are interpreted as the ages of a new magmatic

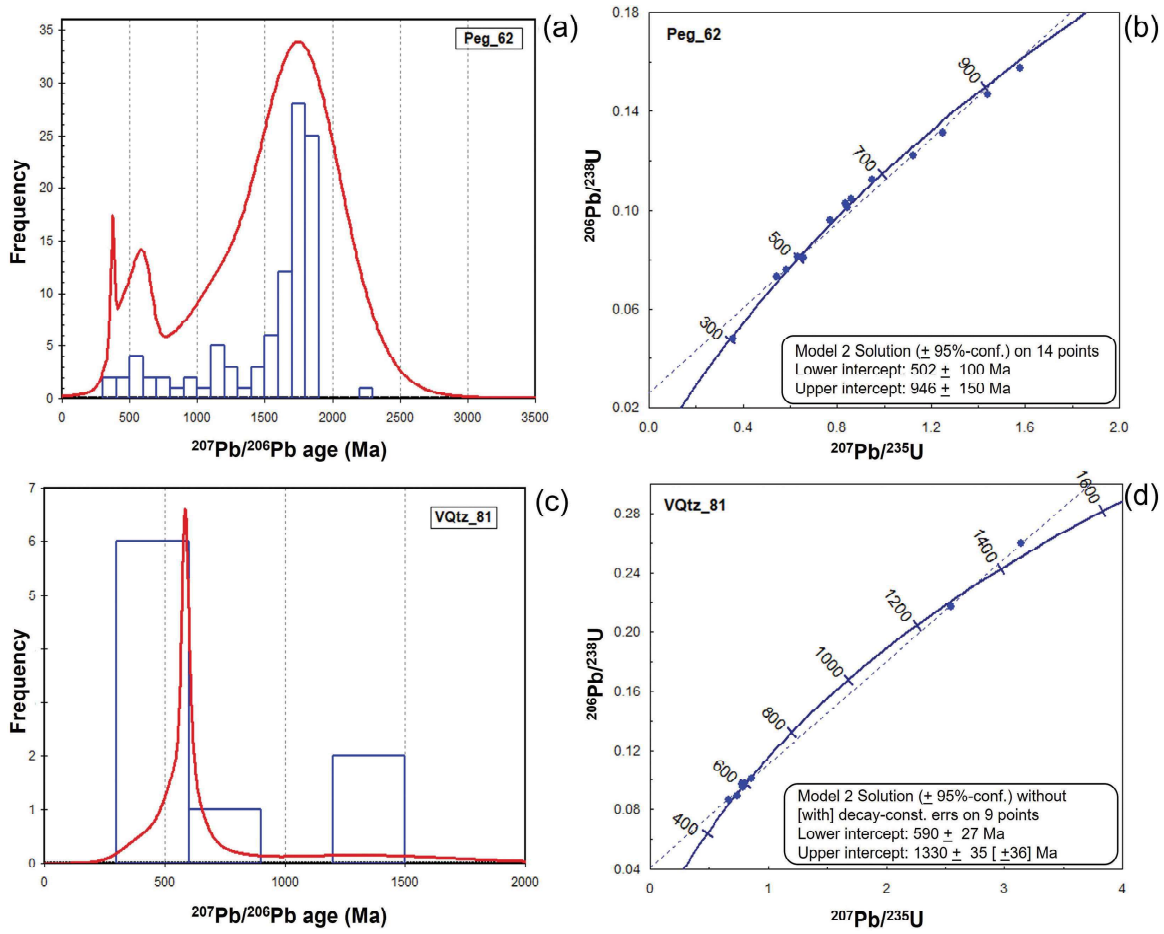


FIGURE 12.10 (a) Probability frequency diagram for zircon ages and (b) $^{206}Pb/^{238}U$ versus $^{207}Pb/^{235}U$ Concordia plot for zircons from pegmatite. (c) Probability frequency diagram for zircon ages and (d) $^{206}Pb/^{238}U$ versus $^{207}Pb/^{235}U$ Concordia plot for zircons from vein quartz.

overgrowth on inherited zircons by partial melting during the Pan-African event. The Concordia plot for the syenite which gave an upper intercept age of 1722+59 Ma (Figure 12.9b) is interpreted as the age of metamorphism of the inherited xenocrystic core on which a new magmatic overgrowth took place at 507+100 Ma (lower intercept age) by partial melting during the Pan-African. The ages obtained for the emplacement of the granodiorite are consistent with the mid-Proterozoic Concordia plot with the upper intercept magmatic age of formation at 1869+87 Ma which was reset by the Pan-African thermotectonic episode as recorded on the lower intercept age of 570+47 Ma (Figure 12.9d).

The $^{206}Pb/^{238}U$ versus $^{207}Pb/^{235}U$ Concordia plot (Figure 12.10b), which yielded an episodically insignificant upper intercept age of 946+150 Ma that was later reset to 502+100 Ma, corresponds to the age of pegmatite late-phase crustal magmatism during the waning stage of the Pan-African dynamo-thermal event as represented in the development of new oscillatory growth on inherited zircons. The Concordia plot (Figure 12.10d) for the vein quartz corresponds to an inherited age of metamorphism that affected the surrounding rocks and a lower intercept age of 590+27 Ma which is interpreted as the time of partial melting and emplacement of the gold-rich quarzitic melt which was remobilized and deposited along major structural trends during the Pan-African. The isochron age of 584 + 49 Ma obtained for the syenogranite is consistent with the $^{206}Pb/^{238}U$ versus $^{207}Pb/^{235}U$ Concordia diagram (Figure 12.11b) with a lower intercept age of 575+17 Ma and an upper intercept age of 2416+360 Ma. While the imprecise upper intercept age (Figure 12.11b) of

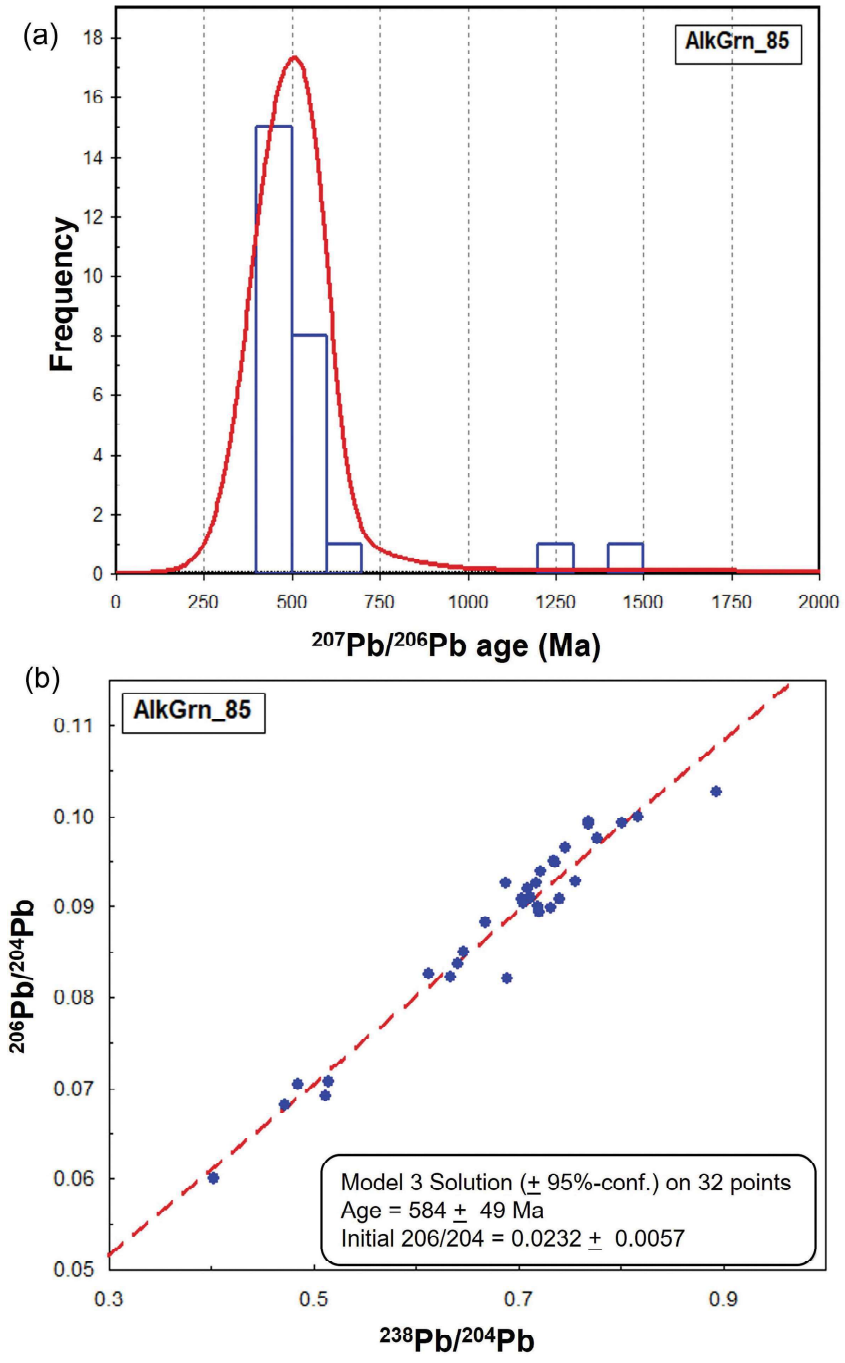


FIGURE 12.11 (a) Probability frequency diagram for zircon ages and (b) $^{206}Pb/^{238}U$ versus $^{207}Pb/^{235}U$ Concordia plot for zircons in syenogranite.

the syenogranite is interpreted as representing an inherited xenocrystic core of a zircon, its lower intercept Pan-African age corresponds to the age of its alkaline magmatic emplacement during the Pan-African. Structural and radiometric age data therefore show that the emplacement of the syenogranite must have contributed to the gold-sulfide-rich hydrothermal fluid which remobilized the gold and deposited it within the regional lineament in Alagbede area.

The similarity between the LA-ICPMS U-Pb zircon crystallization ages of the gold-bearing quartz vein and the immediate felsic igneous rock (vein quartz and syenogranite) suggests that there is a genetic connection between hydrothermal activity and granitic plutonism. The chronological data obtained suggest a temporal link between plutonism and gold metallogeny in the basement complex based on a close spatial relationship between the host granitoids. Alagbede igneous zircons, as indicated by their morphology, oscillatory zoning, and Th/U ratios > 0.1 (Hoskin and Schaltegger et al., 2015; Wu and Zheng, 2004) yielded an age 596 + 28 Ma (Figure 12.11), representing the age of the syenogranite emplacement which triggered off metamorphic dewatering of the gold-bearing surrounding rocks and deposited the sulfide-gold-bearing vein quartz at 590 + 27 Ma (Figure 12.10). This zircon age suggests that the gold mineralization is coeval with the syenogranite in Alagbede. When combined with assay results from residual soil around the rocks (Ajadi et al., 2018), the data suggest two pulses of gold mineralization. The earlier Ashanti-type mineralization in the Paleoproterozoic argillaceous sediments formed by the compressional Birimian event preceded the shield stabilization emplacement of anorogenic granitoids (1900–1700 Ma). It was the earlier orogenic mineralization, which was dispersed during the Pan-African event that was scavenged and reconcentrated by late-phase hydrothermal processes during the Neoproterozoic. The zircon xenocrysts of Archean and Paleoproterozoic ages not only signify the antiquity of the SW Nigerian basement but equally suggest that the gold-bearing mechanism involved the reworking of older Paleoproterozoic (Birimian) disseminated stringers and stockworks in volcano-sediments and granitoids of the compressive Eburnean orogeny while the second was clearly epigenetic and concentrated in hydrothermal vein quartz and stringers during the Pan-African orogeny about 590 ± 27 Ma.

12.4.2 Caveats in the Analytical Methods

Although LA-ICP-MS method for U–Pb age dating of zircon has limitations, mainly arising from the fractionation of U and Pb during ablation, transportation and subsequent ionization, as well as the difficulty to accurately correct for common Pb using ^{204}Pb (i.e., due to ^{204}Hg interference from the He and Ar sample gas used in the ICP-MS) (Frei and Gerdes, 2009), its reliability for U-Th-Pb age dating of igneous, metamorphic and detrital zircon grains has been conclusively demonstrated (e.g., Košler et al., 2002; Jackson et al., 2004; Janoušek et al., 2006; Gerdes and Zeh, 2006; Zeh et al., 2007).

12.4.3 Implication for Gold Mineralization in the Basement Complex of Nigeria

There are practically no constraints on the timing of gold mineralization in Nigeria and the zircon U-Pb data presented here are essentially based on the close association with the contemporaneous zircon-sulfides in the auriferous vein quartz. The data presented form part of a larger database available in Ajadi (2017) and suggest that hydrothermal gold mineralization at the Alagbede deposit corresponds to two phases. An earlier mid-Paleoproterozoic gold mineralization event that was dispersed and later scavenged via hydrothermal fluids responsible for vein-hosted Au–Ag (± Cu, Pb, Zn) mineralization in the Neoproterozoic (mid-late Pan-African). The latter auriferous veins were emplaced following the deformation of the host metasedimentary and metavolcanic rocks (Figure 12.2) described in Ajadi et al. (2018). Most known gold fields in Nigeria occur in proximity to reactivated crustal-scale faults and related structures and are commonly localized within competent, rigid lithological units of granitoid rocks, with some cutting less competent, clastic sedimentary rock sequences (Woakes et al., 1987; Garba, 2000, 2003); the host rocks ranging in age from Late Archean to Neoproterozoic. While the origin of fluids may be varied, the distribution of the mineralization within the Nigerian schist belts in close association with granitoid intrusions suggests that magmatism played a major role in the dynamics of the mineralizing fluids.

12.5 CONCLUSION

The LA-ICPMS U-Pb zircon data combined with the litho-structural study of Alagbede area suggest that the study area is underlain by reactivated Precambrian basement rocks of Archean, Paleoproterozoic and Neoproterozoic ages. It further confirms that southwestern Nigeria is underlain by rocks of great antiquity, comprising early metamorphic tectonites such as migmatitic gneiss, biotite gneiss on which was deposited the older metasediments including quartzite and talc schist, all of which were intruded by the granitoids and late-stage pegmatite and vein quartz in the Pan-African time (Grant, 1970; Oversby, 1975; Pidgeon et al., 1976; Tubosun et al., 1984; Rahaman et al., 1991). The U-Th-Pb chronological data show that the gold deposit in Alagbede area is spatially related to vein quartz formed about 590±27 Ma and fine-grained syenogranite emplacement approximately 575±17 Ma, which are sinistrally sheared by a NW-SE trending fault linked to the Anka-Yauri-Iseyin transcurrent fault. This suggests that the timing of the gold mineralization in Alagbede is related to the formation of structural lineaments linked to the period of felsic magmatism in the study area, the fluids that triggered the gold mineralization have been exsolved from the syenogranite with little contribution from metamorphic dewatering of the quartzite. The broad late Pan-African age of between 617 and 563 (590±27) Ma is hereby proposed as the period of gold mineralization in Alagbede. The concordance between the zircon crystallization ages of the gold-bearing quartz vein and the surrounding felsic igneous rock (syenogranite) suggests a genetic connection between hydrothermal activity and granitic plutonism.

ACKNOWLEDGMENTS

JA is immensely grateful to the Nigerian Tertiary Education Trust Fund for providing part of the funds for this research and to the Nigerian Geological Survey Agency for financial support for the laboratory analysis. The authors wish to thank the staff of the Geoscience Laboratory, University of Witwatersrand, South Africa for making the facilities available. Professors R. Bolhar and G. Bybee are specially appreciated for their close supervision of the various stages of the laboratory work. The authors appreciate the great effort of the three anonymous reviewers that greatly improved this paper.

REFERENCES

Ajadi J, (2017). Geochemistry and Petrogenetic Evolution of Rocks around Bishewa-Ologomo area, part of Lafiagi Sheet 203, Northcentral Nigeria. *International Journal of Scientific and Engineering Research*, 8(4), 1333–1343.

Ajadi, J., Dada, S. S., Nnabo, P., Owoeye, B. A. (2018) Lithostructural description and metalogeny of Alagbede gold deposit West Central Nigeria. *Journal of Environmental & Earth Sciences*, 8(5), 115–132.

Andersen, T. (2002). Correction of common lead in U–Pb analyses that do not report 204Pb. *Chemical Geology*, 192, 59–79. https://doi.org/10.1016/S0009-2541(02)00195-X

Bernet, M., Bassett, K. (2005). Provenance analysis by single-quartz-grain SEM-CL/optical microscopy. *Journal of Sedimentary Research*, 75, 492–500.

Frei, D., Gerdes, A. (2009). Precise and accurate in situ U–Pb dating of zircon with high sample throughput by automated LA-SF-ICP-MS. *Chemical Geology*, 261, 261–270.

Garba, I. (2000). Origin of Pan-African mesothermal gold mineralization at Bin Yauri, Nigeria. *Journal of African Earth Sciences*, 31(2), 433–449.

Garba, I. (2003). Geochemical characteristics of mesothermal gold mineralization in the Pan-African (600±150 Ma) basement of Nigeria. *Applied Earth Science (Transaction of the Institution of Mining and Metallurgy, Section B)*, 112, 319–325.

Gerdes, A., Zeh, A. (2006). Combined U-Pb and Hf isotope LA-(MC)-ICP-MS analyses of detrital zircons: Comparison with SHRIMP and new constraints for the provenance and age of an Armorican metasediment in Central Germany. *Earth and Planetary Science Letters*, 249, 47–61.

Grant, N. K. (1970). Geochronology of Precambrian basement rocks from Ibadan, South-Western Nigeria. *Earth and Planetary Science Letters*, 10, 29–38.

Jackson, S., Pearson, N. J., Griffin, W. L., Belousova, E. A. (2004). The application of laser ablation - inductively coupled plasma - mass spectrometry to in situ U-Pb zircon geochronology. *Chemical Geology*, 211, 47–69.

Janoušek, V., Gerdes, A., Vrána, S., Finger, F., Erban, V., Friedl, G., Braithwaite, C. J. R. (2006). Low-pressure granulites of the Lišov Massif, Southern Bohemia: Viséan Metamorphism of Late Devonian Plutonic Arc Rocks. *Journal of Petrology*, 47, 705–744.

Košler, J., Fonneland, H., Sylvester, P., Tubrett, M., Pedersen, R. B. (2002). U-Pb dating of detrital zircons for sediment provenance studies-a comparison of laser ablation ICPMS and SIMS techniques. *Chemical Geology*, 182, 605–618.

Mezger, K., Krogstad, E. J. (1997). Interpretation of discordant U-Pb zircon ages: An evaluation. *Journal of Metamorphic Geology*, 15, 127–140.

Oversby, V. M. (1975). Lead Isotope study of aplites from the Precambrian rocks near Ibadan, southwestern Nigeria. *Earth and Planetary Science Letters*, 27, 177–180.

Pidgeon, R. T., Van Breeman, O., Oyawoye, M. O. (1976). Pan African and earlier events in the basement complex of Nigeria. In *25th International Geological Congress Australia*, Abstr., 3 p., 667.

Rahaman, M. A., Emofurieta, W. G., Vachette, M. C. (1983). The potassic granites of Igbeti area: Further evidence of the polycyclic evolution of the Pan-African belt in Southwestern Nigeria. *Precambrian Research*, 22, 75–92.

Rahaman, M. A., Tubosun, I. A., Lancelot, J. R. (1991). U-Pb geochronology of potassic syenites from southwestern Nigeria and the timing of deformational events during the Pan-African orogeny. *Journal of African Earth Sciences*, 13, 387–395.

Schaltegger, U., Schmitt, A. K., Horstwood, M. S. A. (2015). U-Th-Pb zircon geochronology by ID-TIMS, SIMS, and laser ablation ICP-MS: Recipes, interpretations, and opportunities. *Chemical Geology*. doi: 10.1016/j.chemgeo.2015.02.02.

Tubosun, I. A., Lancelot, J. R., Rahaman, M. A., Ocan, O. (1984). U–Pb Pan-African ages of two charnockite-granite association from southwestern Nigeria. *Contribution to Mineralogy and Petrology*, 88, 188–195.

Woakes, M., Rahaman, M. A., Ajibade, A. C. (1987). Some metallogenetic features of the Nigerian basement. *Journal of African Earth Sciences*, (1983) 6, 655–664. https://doi.org/10.1016/0899-5362(87)90004-2

Wu, Y. B., Zheng, Y. F. (2004). Genesis of zircon and its constraints on interpretation of U-Pb age. *Chinese Science Bulletin*, 49, 1554–1569.

Zeh, A., Gerdes, A., Klemd, R., Barton Jr., J. M. (2007). Archean to Proterozoic crustal evolution in the Central Zone of the Limpopo Belt (South Africa/Botswana): Constraints from combined U-Pb and Lu-Hf isotope analyses of zircon. *Journal of Petrology*, 48, 1605–1639.